Proceedings of the 38th Engineering Geology & Geotechnical Engineering Symposium
Edited by Elfass, Norris and Watters, University of Nevada, Reno, 2003

Healing of Rock Salt Fractures

K. Fuenkajorn, D. Phueakphum and M. Jandakaew
Geological Engineering Program
Suranaree University of Technology
111 University Avenue, Muang District
Nakhon Ratchasima 30000, THAILAND

ABSTRACT

Healing effectiveness of fractures in rock salt has been assessed experimentally in terms of stress states, fracture types, and time. Tension-induced fractures and fractures formed by saw-cut surfaces and by polished surfaces have been tested. Series of gas flow testing measure the changes of the fracture permeability under pressurization. All tests are conducted at room temperature. Brazilian tensile strengths and point load strengths are used as an indicator of the healing effectiveness. The results suggest that the primary factors governing the healing of salt fractures are the origin and purity of the fractures, and the magnitudes and duration of the fracture pressurization. The hydraulic conductivity for all salt fractures decreases with increasing pressure and time. The reduction of fracture permeability due to the closure does not necessarily mean that the healing has occurred. The fracture closure can enhance the fracture healing. Both processes are time-dependent. The closure involves the visco-plastic deformation of the salt on both sides of the fracture. Under preferable conditions and environment, a complete healing of rock salt fractures is possible.

1. INTRODUCTION

It is defined here that healing is the closure of fractures without any precipitation of materials inside. It is a chemical and physical process in which the material properties evolve with time or in which the defects (voids and cracks) decrease. Healing of rock fractures may occur on various scales. In geology, fracture healing is an important mechanism controlling the circulation of fluid in the earth crust. This process can change the fluid circulation and interactions between the lower crust and the surface. In a smaller scale, circulation of solution or fluid in rock mass can result in a precipitation or deposition of minerals and ores in fracture zones. The factors that may affect the rate of crack healing are time, stress, temperature, saturation, geometry of contact surfaces, and chemical alterations (Renard, 1999).

Healing of fractures in rock salt formations can prevent brine flow from contaminating the upper surface or nearby rock formations. Damage in rock salt can be healed under hydrostatic and non-hydrostatic compression. When cracks are closed, permeability can be reduced by several orders of magnitude. The healing capability of fractures is one of the advantages for rock salt to

be used as a host rock for nuclear waste repository in the United States and Germany (Habib and Berest, 1993). The presence of damage in the form of micro-cracks in salt can alter the structural stability and permeability of salt, affecting the integrity of a repository (Chan et al., 1998). The healing of rock salt fractures around the air or gas storage caverns also affects the designed storage capacity and the mechanical stability of the caverns (Katz and Lady, 1976). Miao et al. (1995) state that healing of rock salt is probably due to the visco-plastic deformation of grains, causing the closure of cracks and pore spaces. The size reduction of the micro-cracks can increase the salt stiffness and strength. The main driving force for fracture healing is a minimization of surface tension, and creation of contact areas and covalent bonds between the two surfaces of the fracture.

Even though the initiation, propagation and healing of fractures in salt mass around underground structures have long been recognized, most investigations have been concentrated on their impact on the mechanical constitutive behavior of the rock (e.g., Allemandou and Dusseault, 1993; Munson et al., 1999). Several experimental researches on the healing and consolidation of crushed salt have also been carried out in an attempt at understanding the healing behavior between the salt particles and their impact on the bulk properties (e.g., Ouyang and Daemen, 1989; Miao et al., 1995). A direct experimental assessment of the healing behavior of individual salt fractures remains rare.

The objective of the research presented here is to determine experimentally the healing effectiveness of rock salt fractures as affected by the stress conditions, fracture types, and time. The effort involves healing tests under uniaxial and radial pressures, gas flow permeability tests to monitor the time-dependent behavior of the salt fractures, and point loading and diameter loading tests to assess the mechanical performance of the fractures after healing.

2. BASIC PROPERTIES OF SALT SPECIMENS

The basic characterization tests on salt have been carried out. They include uniaxial compressive strength testing, Brazilian tensile strength testing and point load strength index testing. These tests yield the strength properties needed for designing the healing test parameters. The salt specimens have been drilled from the Middle and Lower members of the Maha Sarakham Formation in the Sakhon Nakhon Basin, northeastern Thailand. Suwanich (1986), Utha-aroon et al. (1995) and Warren (1999) give detailed descriptions of the salt and the geology of the basin. The core specimens are from the depths ranging between 250 and 400 meters. The nominal core diameter is 60 mm. They are cut and polished to specific dimensions for each test. The sample preparation and test procedures follow as much as practical the ASTM standard practices (i.e., ASTM D2938, D3967, D4543 and D5731). Table 1 summarizes the characterization test results. The salt strengths are relatively high as compared with those from other sources in the United States, Canada and Germany. This is due to the significant amount of inclusions, such as anhydrite, sulfates, carbonates, and iron oxides.

Table 1 Summary of characterization test results.

Salt Unit	Depth (m)	Test Methods		
		Uniaxial Strength, σ_c	Brazilian Strength, σ_B	Point Load Strength, I_s
Middle Salt	252 - 329	30.2 ± 4.2 MPa	1.9 ± 0.3 MPa	1.0 ± 0.01 MPa
Lower Salt	390 - 410	31.1 ± 6.7 MPa	1.7 ± 0.3 MPa	0.6 ± 0.05 MPa

3. FRACTURE HEALING EXPERIMENTS

Two test schemes are proposed to assess the healing behavior of the salt fractures: healing under uniaxial (normal) loading and healing under radial loading. All tests are conducted under isothermal conditions (20-25°C). Three types of salt fracture have been simulated in the laboratory: 1) tension-induced fractures, 2) fractures formed by saw-cut surfaces, and 3) fractures formed by smooth polished surfaces. Salt surfaces on both sides of the fracture are well mated. The salt specimens are prepared to have a diameter of 60 mm with a length-to-diameter ratio of 2.5. To obtain the tension-induced fractures, the cylindrical specimens are subjected to point loading or by diameter loading (Brazilian tension test). The point-loaded fracture is normal to the specimen axis, and is prepared for healing under uniaxial loading. The diameter-loaded fracture is the axial fracture, parallel to the specimen axis, and will be healed under radial loading. The fracture formed by saw-cut surfaces is also normal to the specimen axis, while the fracture formed by polished (grinding) surfaces is parallel to the specimen axis. After the fractures have been prepared, the amount of inclusions on the fracture surfaces is measured and mapped using magnifying glass. The aerial percentage of the inclusions is calculated with respect to the total fracture area. The inclusions defined here are all associated and foreign minerals or materials that are not sodium chloride. Prior to the healing test, a close examination is made to determine whether the tension-induced fractures are formed by the splitting failure of the salt crystals or by the separation of the inter-crystalline boundaries.

3.1 Healing under Normal Loading

Table 2 shows the test matrix for the healing test under uniaxial loading. Four test series with different test conditions have been performed. For the first two series, low normal stresses of 3.2 kPa and 3.8 kPa are applied to the saw-cut surfaces under dry and saturated conditions. Three specimens are used for each normal stress. Dead weight machine applies constant loading on to the fracture. For the saturated condition, the fractures are submerged under saturated brine while loading. The load is removed after testing for 30 days. No healing has been observed for both dry and saturated fractures. All saw-cut fractures remain separable.

The third and fourth test series use a normal stress of 4.3 MPa on three saw-cut fractures, and 7.8 MPa on ten tension-induced fractures. Figures 1 and 2 show some salt specimens prepared for these test series. A consolidation machine with the maximum load capacity of 2 tons is used to apply constant stresses to the specimens (Figure 3). The specimens are unloaded after 30 days.

Table 2 Summary the healing tests scheme for uniaxial loading.

Test Methods	Fracture Characteristics		Number of Specimens	Test Conditions
Uniaxial Loading	Normal Fracture	Saw-cut surface	3	*Series 1* - σ_{axial} = 3.2 kPa - dry condition - 30 days
			3	*Series 2* - σ_{axial} = 3.8 kPa - saturated condition - 30 days
			3	*Series 3* - σ_{axial} = 4.3 MPa - dry condition - 30 days
		Tension-induced fracture by point loading	10	*Series 4* - σ_{axial} = 7.8 MPa - dry condition - 30 days - percentage of inclusions varies from 0 to 40%

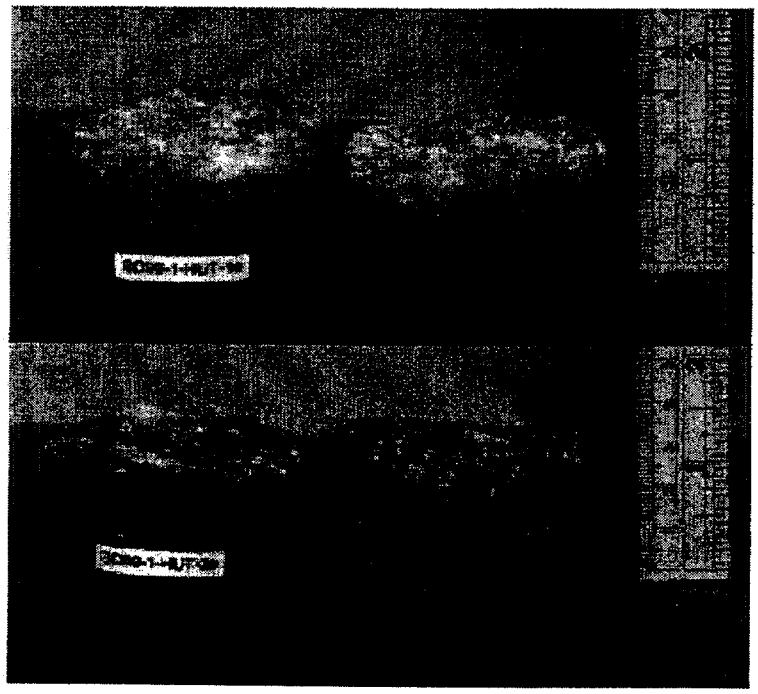

Figure 1 Some salt specimens with normal fractures formed by tension-induced fractures normal to specimen axis. Top: fractures with no inclusion. Bottom: fractures with 30% inclusion.

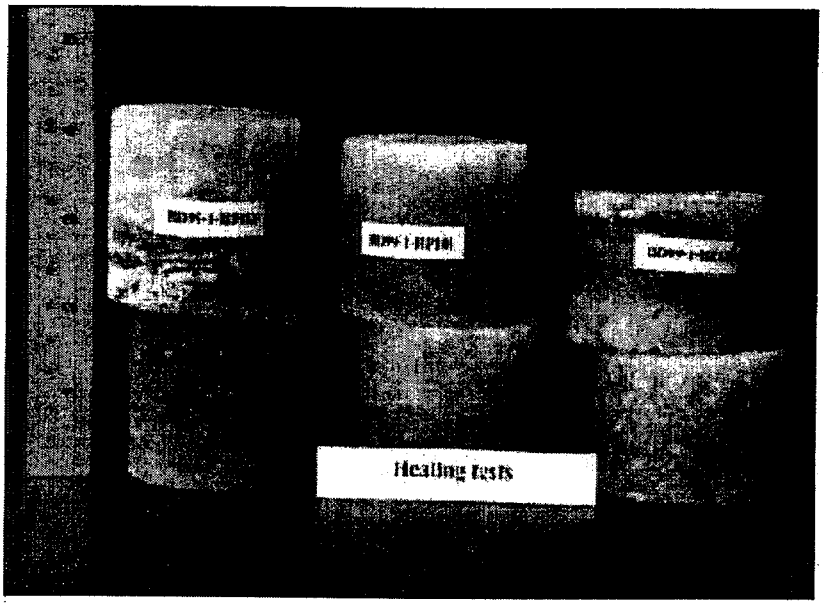

Figure 2 Some salt specimens with normal fractures formed by saw-cut surface prepared for healing under uniaxial loading.

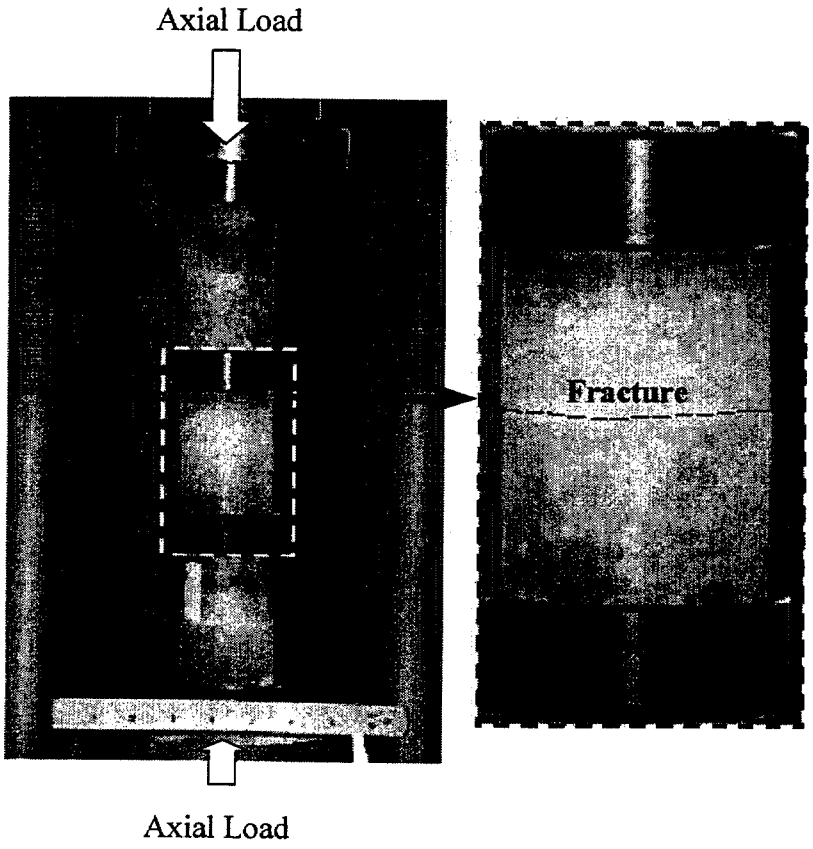

Figure 3 Healing test under uniaxial loading. The specimens are loaded axially by means of dead weight consolidation machine

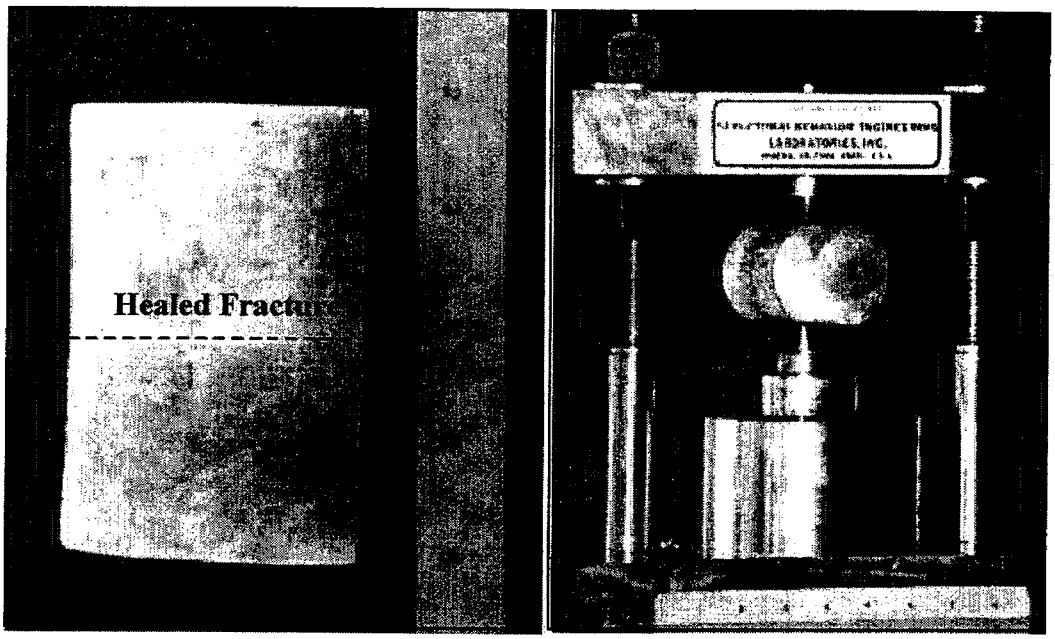

(a) (b)

Figure 4 Salt specimen with fracture after healing under uniaxial load (left). The healing effectiveness is assessed by point load testing (right).

In order to assess the healing effectiveness, the specimens are subjected to point load testing by having the loading points lied on and parallel to the healed fracture plane (Figure 4). The point load strength of the healed fracture (I_H) is calculated by dividing the failure load (P) by the diameter square (D^2). The healing effectiveness (H_e) of each fracture is defined by the percentage ratio of the I_H to I_S, where I_S represents the point load strength of the intact salt obtained previously from inducing the fracture to the same specimen. All specimens fail along the original fracture plane.

No healing has been detected on the fractures formed by saw-cut surfaces tested under 4.3 MPa normal stress (test series 3). Healing however has been observed on the tension-induced fractures tested under 7.8 MPa normal stress (test series 4). Table 3 summarizes the results. Some H_e values exceed 100%. This is probably because some existing voids or fissures in salt along the fracture plane are compressed during healing period, and subsequently strengthening the fracture beyond the previous intact condition. It should be noted that before the fractures are initially induced, the intact core specimens have not been subjected to any compression. The high variation of H_e values may be also due to the accuracy of the testing technique. Even though assessment of healing effectiveness by point load testing is relatively quick and easy, the high stress gradient induced in the specimen usually results in a high intrinsic variability of the measurement results. The complex distribution, pattern and locations of the inclusions in relation to the loading points can also enhance the variability of the strength results. The healing effectiveness tends to decrease as the amount of inclusion increases. However, their mathematical relationship can not be constructed due to the high variation of the results.

Table 3 The point load test results for dry salt specimens with tension-induced fractures after healing under constant axial stress of 7.8 MPa for 30 days.

Specimen No.	Percentage of Inclusions (%)	Point Load Strength Index		Healing Effectiveness $H_e=[I_H/I_S]\times100$ (%)
		Intact Salt, I_S (MPa)	Salt with Healed Fracture, I_H (MPa)	
HUT01e	0	0.61	1.13	185
HUT02e	30	1.05	0.75	71
HUT03e	5	0.84	1.00	119
HUT04e	40	1.09	0.40	37
HUT05e	25	0.87	0.74	85
HUT06e	10	0.56	0.59	105
HUT07e	5	1.22	0.49	40
HUT08e	5	1.25	0.48	38
HUT09e	25	0.54	0.51	94
HUT10e	15	0.56	0.40	71

3.2 Healing under Radial Loading

Tension-induced fractures and the fractures formed by polished surfaces are subjected to healing test under radial loading. Figure 5 shows the axial fracture in the salt specimen. The "Overburden Poro-Perm Cell" applies constant radial pressures to the salt specimen (Figure 6). It is capable of applying radial pressure up to 70 MPa. No axial stress is applied on the specimen. Each fracture type is subjected to two loading configurations: single-step loading and multi-step loading. Table 4 summarizes the test matrix. All specimens are tested under dry condition. During pressurization, gas flow permeability test is performed. The measured flow rate is used to calculate the hydraulic conductivity of the fracture (K_f), based on an assumption of the flow through parallel plates (Zeigler, 1976). It is assumed that the fracture width equals the specimen diameter, and the length equals the specimen length. The nitrogen gas pressure is injected at a constant magnitude of 0.35 MPa. The measurement limit of the system is about 10^{-8} m/s.

One polished fracture is subjected to the radial pressures (P_c) of 3.45 MPa and later increased to 6.89 MPa (multi-step loading). Each loading step takes 100 hours. This pressure scheme is repeated for the second cycle. Figure 7 shows the flow test results during the pressurization. The fracture permeability decreases with increasing the radial pressures. Under each pressure, the fracture permeability also decreases as the testing time increases. The second cycle of pressurization yields a lower hydraulic conductivity than do the first one. When the pressure increases to 6.89 MPa, the hydraulic conductivity becomes lower than the limit of measurement (10^{-8} m/s). This suggests that a plastic closure of the fracture has occurred. The fracture has undergone a permanent deformation.

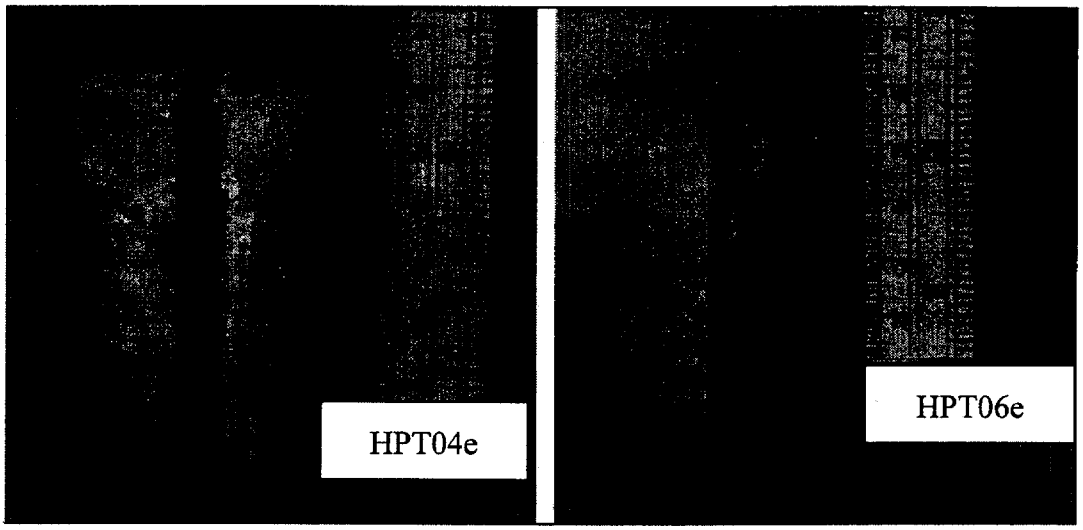

(a) (b)

Figure 5 A specimen with tension-induced fractures is prepared by diameter loading (a). A specimen with polished fracture (b). They are prepared for gas flow permeability testing.

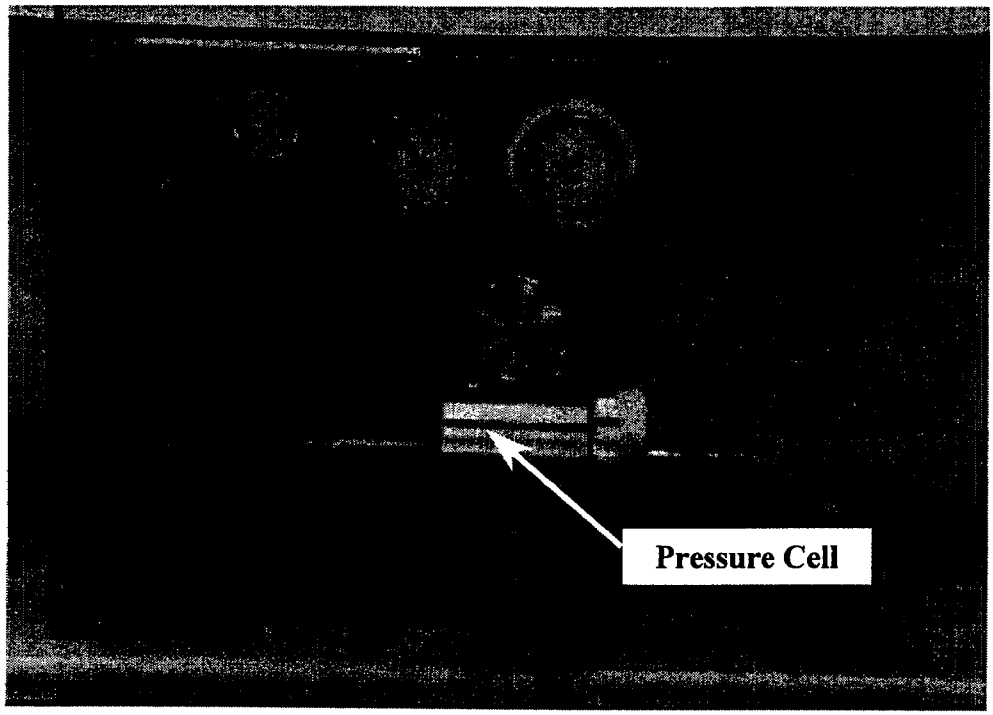

Figure 6 Gas flow permeability test using "Overburden Poro-Perm Cell". The salt specimen is subject to radial loading between 0.69 and 20.67 MPa in the pressure cell.

Table 4 Summary the healing tests scheme for radial loading.

Test Methods	Fracture Characteristics		Number of Specimens	Test Conditions
Radial Loading	Axial Fracture	Polished surface	1	*Multi-step Loading* - $P_c = 3.45 \rightarrow 6.89$ MPa - 100 hours/step - dry condition - two loading cycles
		Tension-induced fracture by diameter loading	5	*Single-step Loading* - $P_c = 0.69$, 3.45, 6.89, 13.78, and 20.67 MPa - 120 hours - dry condition
			3	*Multi-step Loading* - $P_c = 3.45 \rightarrow 6.89 \rightarrow 10.34 \rightarrow 13.78$ MPa - 96 hours/step and 24 hours/step - dry condition - two loading cycles.

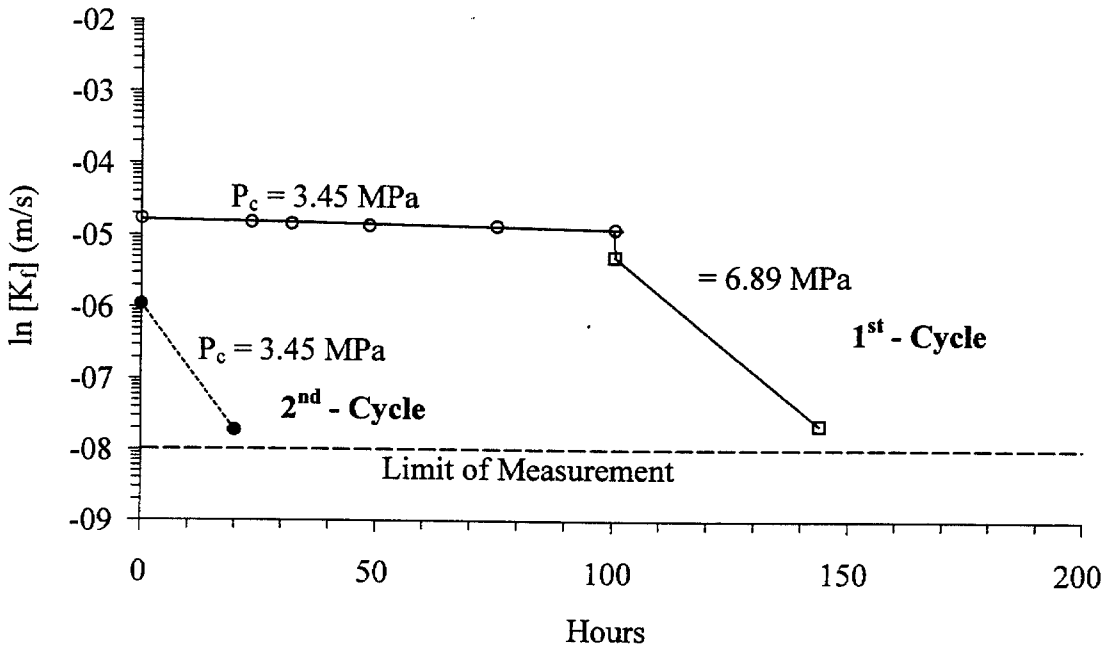

Figure 7 Hydraulic conductivity (K_f) of the specimen with polished surface as a function of time under multi-step radial loading. Two loading cycles are presented for specimen no. HPT06e.

Three specimens with tension-induced fracture are tested under multi-step loading. The pressure are progressively increased from 3.45, 6.89, 10.34 to 13.78 MPa. The reduction of fracture permeability with increasing time and pressurization tends to be greater than that of the polished fracture. The fracture permeability obtained from the second pressure cycle is notably lower than that of the first cycle, suggesting a significant closure of the fracture (Figures 8 through 10). The closure is also plastic (permanent) and time-dependent.

For the single-step loading, five specimens subject to constant radial pressures of 0.69, 3.45, 6.98, 13.78 and 20.67 MPa. This test series is aimed at determining the rate change of the fracture permeability with time. A power equation is used to fit the experimental results for each pressure level: $K_f = K_o (t)^{-\beta}$, where K_o represents the fracture permeability at time equal to 1, and β is the time coefficient (Figure 11). The time coefficient β increases exponentially with the applied pressure (P_c): $\beta = 0.104 \cdot \exp(0.14\ P_c)$. This suggests that the reduction rate of fracture permeability is higher when the fracture subjects to a greater pressure.

It is visually observed that healing has occurred on all fractures after 120 hours of radial pressurization. Figure 12 shows a salt specimen with tension-induced fracture before and after healing. The Brazilian tensile strengths of each specimen conducted before and after healing are compared to assess the healing effectiveness (H_e) of the fracture. Here H_e represents the percentage ratio of the fracture tensile strength (σ_H) to the intact tensile strength (σ_B) of the same salt specimen. The tensile failure occurs along the same plane that was induced before and after healing. Tables 5 and 6 summarize the results of the healing assessment test. They suggest that the polished fractures can not be effectively healed even under the radial pressure of 6.89 MPa for 120 hours. Healing however can be clearly measured for the tension-induced fractures. Figure 13 shows the increase of H_e as the radial pressure (P_c) increases for the single-step loading on the tension-induced fractures.

4. DISCUSSIONS AND CONCLUSIONS

Fracture healing under radial loading has an advantage over that under uniaxial loading, in term of the maximum applied pressures. The applied load is limited by the compressive strength of the salt. The maximum axial stress used here is therefore limited to 7.8 MPa or about 30% of the strength. This is primarily to prevent the initiation of micro-cracks or fractures in the intact salt. For the radial loading, the specimen can subject to the pressure as high as 20 MPa. The results suggest that both applied pressure and time are important factors for fracture healing.

The healing effectiveness of salt fractures depends heavily on the origin of the fractures. If a fracture is formed by the separation or splitting of salt crystals, it can be easily healed even under relatively low stress for a short period. The splitting failure of salt crystals occurs by a separation of cleavage planes. This means that healing is effective if the salt crystals on both sides of the cleavage plane return to their original position. For the fractures formed by separation of inter-crystalline boundaries or by crystals with different orientations on the opposite sides, healing will not be easily achieved. In particular, if the fracture surface is coated

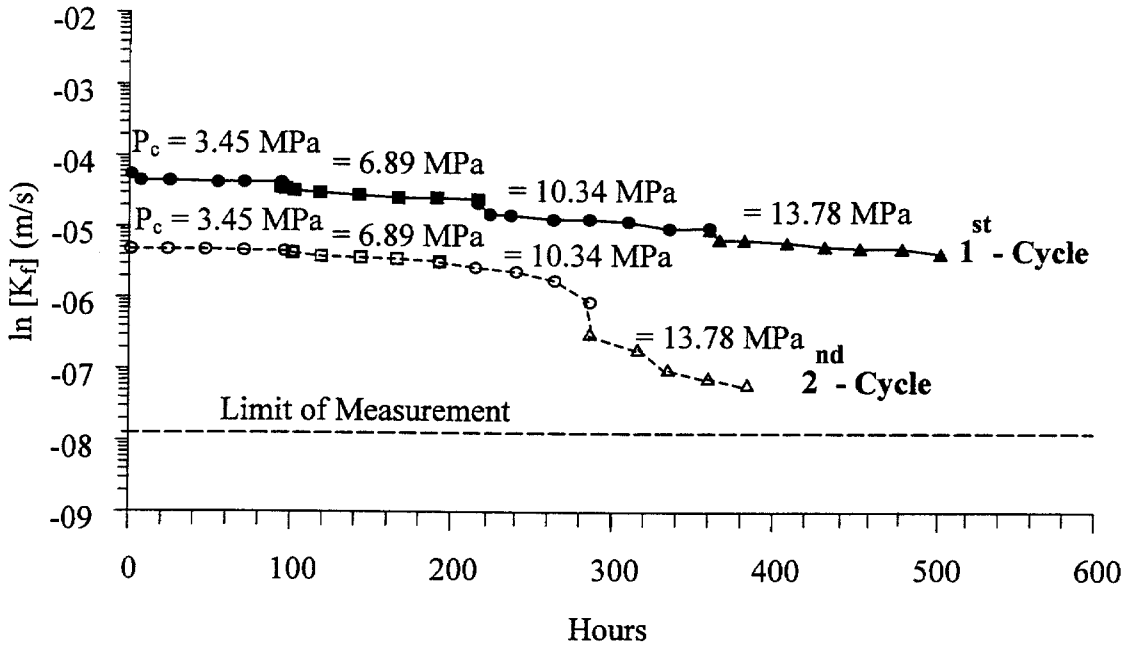

Figure 8 Hydraulic conductivity (K_f) of the specimen with tension-induced fracture as a function of time under multi-step radial loading. Two loading cycles are presented for specimens no. HPT07e.

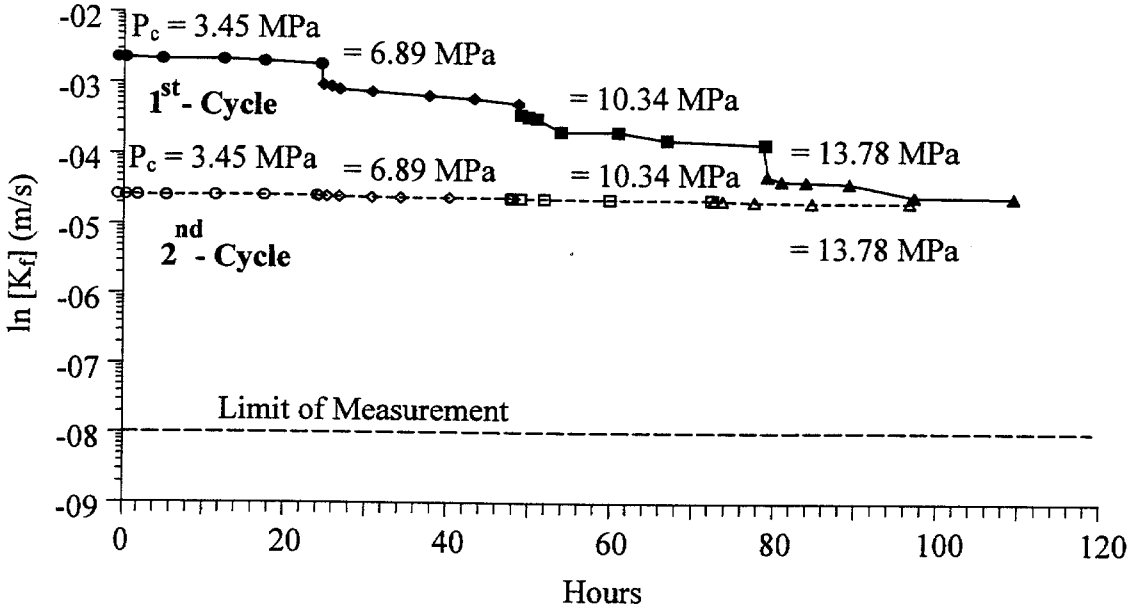

Figure 9 Hydraulic conductivity (K_f) of the specimen with tension-induced fracture as a function of time under multi-step radial loading. Two loading cycles are presented for specimens no. HPT08e.

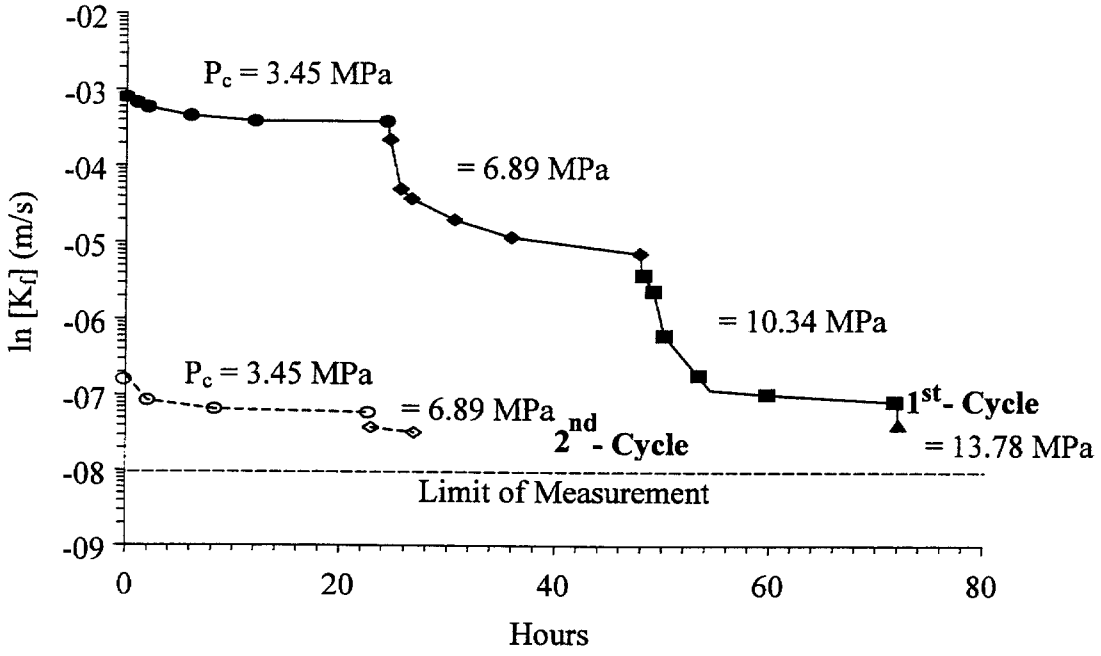

Figure 10 Hydraulic conductivity (K_f) of the specimen with tension-induced fracture as a function of time under multi-step radial loading. Two loading cycles are presented for specimens no. HPT09e.

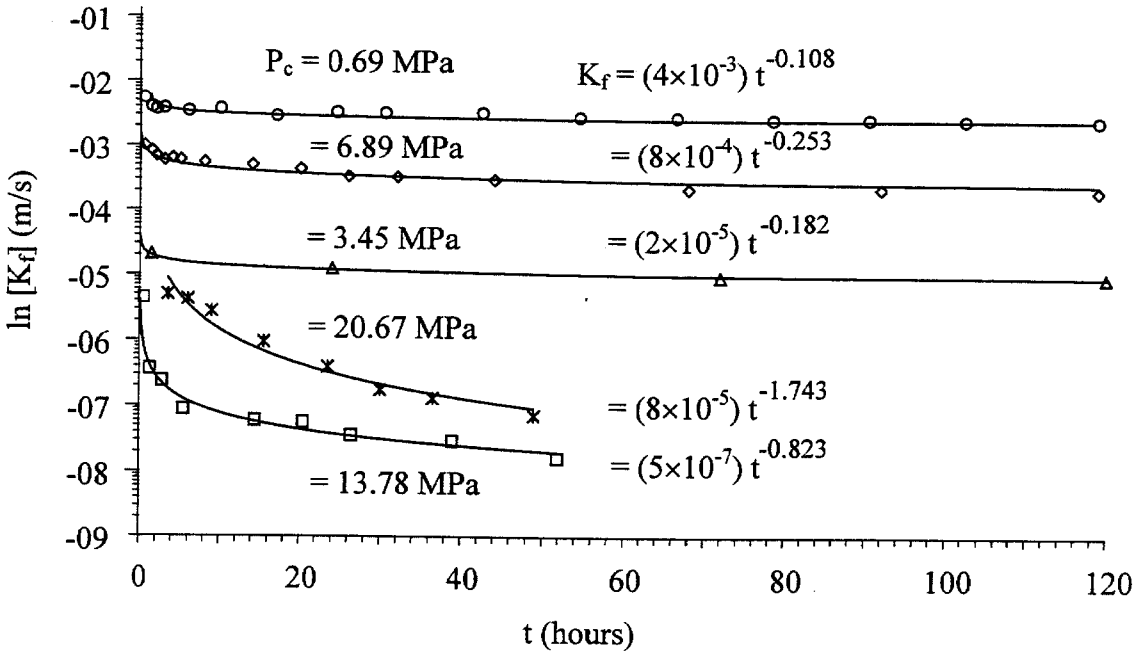

Figure 11 Hydraulic conductivity (K_f) of tension-induced fractures as a function of time under single-step radial loading. Five specimens are tested with different radial pressures (P_c).

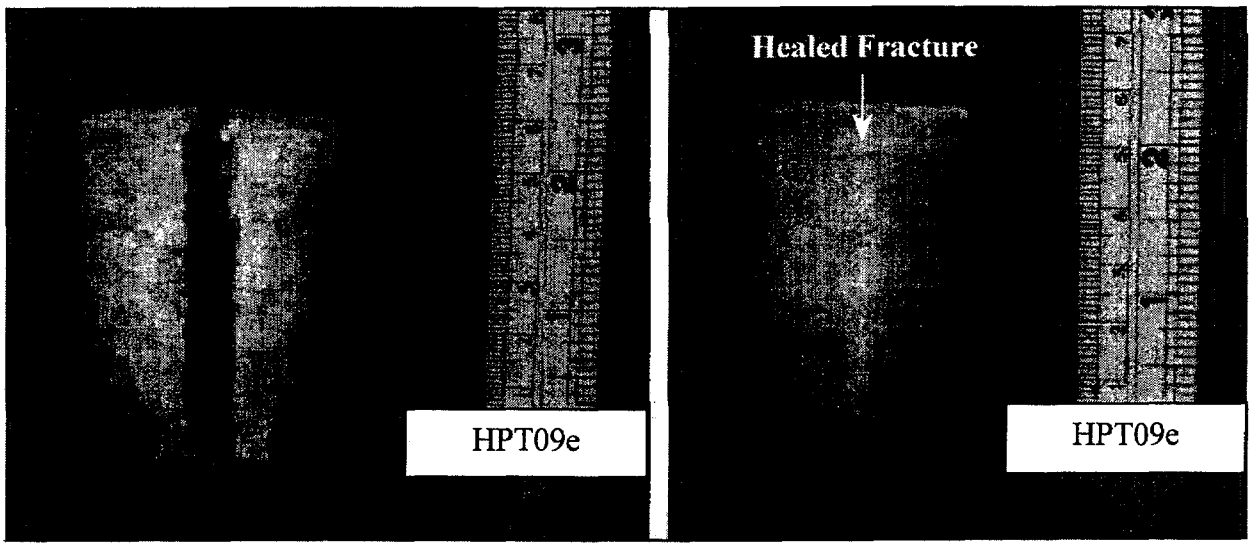

(a) (b)

Figure 12 The specimen with tension-induced fractures are prepared by diameter loading, before healing (a), and after healing (b).

Table 5 The Brazilian tension test results for dry salt specimens with tension-induced fractures and polished surfaces after healing under single-step radial loading for 120 hours.

Specimen No.	Type of Fracture	Radial Pressure (MPa)	Brazilian Tensile Strength		Healing Effectiveness $H_e = (\sigma_H/\sigma_B)\times 100$ (%)
			Intact Salt, σ_B (MPa)	Salt with Healed Fracture, σ_H (MPa)	
HPT01e	Tension-induced fracture	0.69	2.24	0.04	2
HPT02e		3.45	2.23	0.37	17
HPT03e		6.89	2.24	0.36	16
HPT04e		13.78	2.47	1.04	42
HPT05e		20.67	1.96	0.82	42

Table 6 The Brazilian tension test results of dry salt specimens with tension-induced fractures and polished surfaces after healing under multi-step radial loading for 120 hours.

Specimen No.	Type of Fracture	Radial Pressure (MPa)	Test Duration	Brazilian Tensile Strength		Healing Effectiveness $H_e = (\sigma_H/\sigma_B)\times100$ (%)
				Intact Salt, σ_B (MPa)	Salt with Healed Fracture, σ_H (MPa)	
HPT06e	Polished surface	3.45 → 6.89	100 hrs/step	1.68	0.06	4
HPT07e	Tension-induced fracture	3.45 → 6.89 → 10.34 → 13.78	96 hrs/step	1.30	1.24	94
HPT8e			24 hrs/step	2.50	1.97	79
HPT09e				2.23	1.17	53

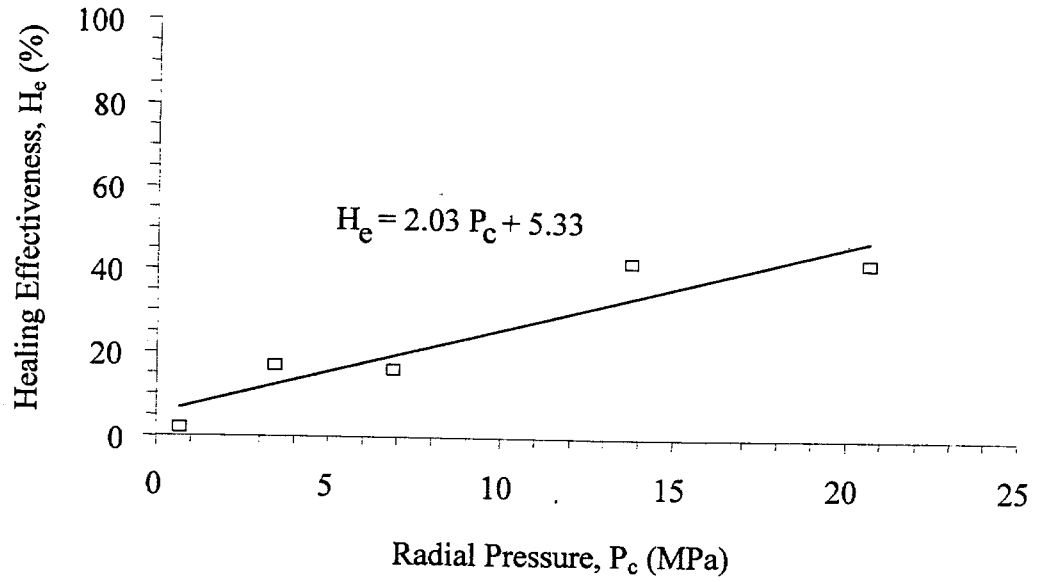

Figure 13 Healing effectiveness (H_e) as a function of radial pressure (P_c) for specimens with tension-induced fracture after healed for 120 hours.

with any inclusions, healing will not occur. This explains why the saw-cut fractures and polished fractures can not be effectively healed under the test conditions used here. It can be postulated here that healing of fracture can be enhanced by the purity of the halite crystals on the opposite sides of the fracture. This is supported by the fact that the cleavage planes inside the salt crystal are more pure than the inter-crystalline boundaries, and more than the saw-cut and polished surfaces. These artificial surfaces could be contaminated during the preparation process. To heal a saw-cut or polished salt fracture, a much higher confinement and temperature than those used here may be required.

It is not clear from the experimental results that fractures under saturated brine can be healed more effective than those under dry condition. This is because the two test conditions are used on the saw-cut fractures and with a relatively low axial stress. For the saturated testing, it is found that re-crystallization of brine between the fractures has occurred in form of small salt crystals. Such process however can not hold the fractures together. The specimens can be easily pulled apart by hands.

The hydraulic conductivity for all salt fractures decreases with increasing applied pressure and time. This implies that the fracture healing is accompanied by the fracture closure. Both processes are time-dependent. The closure involves the visco-plastic deformation for the salt on both sides of the fracture. The healing involves a chemical process. It is permanent - remains even after the load is removed. Owing to the surface smoothness, the polished fractures show a lower permeability than do the tension-induced fractures. This however does not necessarily mean that the polished fractures heal more effective than do the tension-induced fractures. A reduction of fracture permeability does not necessarily mean that the healing has occurred. This is evidenced by that even the polished fracture has been compressed until its permeability becomes lower than 10^{-8} m/s, no healing has taken place in the fracture.

Since all fractures tested here are well mated, the impact of fracture roughness can not be truly assessed. More testing is needed to confirm any mathematical relationship between the healing effectiveness and the inclusions. For the healing assessment method, a direct tension test could be used to minimize the impact of the stress gradient induced along the fracture plane. From the results obtained here, it can be postulated that under preferable conditions (stress state, time, temperature, purity, crystal orientation, etc.), a complete healing of salt fractures is possible.

5. REFERENCES

Allemandou, X. and M.B. Dusseault, 1993, "Healing processes and transient creep of salt rock," *Geotechnical Engineering of Hard Soils-Soft Rocks*, Balkema, Rotterdam, pp. 1581-1590.

ASTM D2938-79, Standard test method for unconfined compressive strength of intact rock core specimens. *Annual Book of ASTM Standards*, 04.08, American Society for Testing and Materials, Philadelphia.

ASTM D3967-81, Standard test method for splitting tensile strength of intact rock core specimens. *Annual Book of ASTM Standards*, 04.08, American Society for Testing and Materials, Philadelphia.

ASTM D4543-85, Standard practice for preparing rock core specimens and determining dimensional and shape tolerances. *Annual Book of ASTM Standards*, 04.08, American Society for Testing and Materials, Philadelphia.

ASTM D5731-95, Standard test method for determination of the point load strength index of rock. *Annual Book of ASTM Standards*, 04.08, American Society for Testing and Materials, Philadelphia.

Chan, K. S., D. E. Munson, A. F. Fossum, and S. R. Bodner, 1998, A constitutive model for representing coupled creep, fracture and healing in rock salt, *Proceeding of the 4th Conference on the Mechanical Behavior of Salt*, The Pennsylvania State University, June 17-18, 1996, Clausthal-Zellerfeld, Trans Tech Publications, Germany, pp. 211-234.

Habib, P. and P. Berest, 1993, Rock mechanics for underground nuclear waste disposal in France, *Comprehensive Rock Engineering*: Developments and case studies: Geothermal Energy and Radioactive Waste Disposal, Vol. 5, Great Britain: Pergamon, pp. 547-563.

Katz, D. L. and E. R. Lady, 1976, *Compressed Air Storage for Electric Power Generation*, Richland, Washington Dept. of Energy, Pacific Northwest.

Miao, S., M. L. Wang, and H. L. Schreyer, 1995, Constitutive models for healing of materials with application to compaction of crushed rock salt, *Journal of Engineering Mechanics*, ASCE., Vol. 10, No. 121, pp. 1122-1129.

Munson, D.E., K.S. Chan and A.F. Fossom, 1999, *Fracture and Healing of Rock Salt related to Salt Caverns*, SMRI Report, Spring Meeting, Solution Mining Research Institute, Encinitas, California, April 14-16, Las Vegas, Nevada.

Ouyang, S. and J.J.K. Daemen, 1989, *Crushed Salt Consolidation*, Technical Report NUREG/CR-5402, U.S. Nuclear Regulatory Commission, Washington, DC.

Renard, F., 1999, *Pressure Solution and Crack Healing and Sealing*, Geology related to nuclear waste disposal, Institute of Geology and Department of Physics. Roztez, Norway: Czech Republic. 32pp.

Suwanich, P., 1986, Potash and rock salt in Thailand. *Nonmetallic Minerals Bulletin No. 2*, Economic Geology Division, DMR, Bangkok, Thailand.

Utha-aroon, C., L. Coshell and J.K.Warren, 1995, Early and late dissolution in the Maha Sarakham Formation: Implications for basin stratigraphy, *Int. Conf. On Geology, Geotechnology and Mineral Resources of Indochina (GeoIndo'95)*, November 22-25, pp. 275-286.

Warren, J., 1999, *Evaporites: Their Evolution and Economics*. Blackwell Science, 438 pp.

Zeigler, T.W., 1976, *Determination of Rock Mass Permeability*, Technical Report S-76-2, U.S. Army Engineer Waterways Experiment Station, Vicksburg, Mississippi.

6. ACKNOWLEDGEMENTS

Suranaree University of Technology has provided funding for this research. Permission to publish this paper is gratefully acknowledged. We would like to thank Asia Pacific Potash Corporation, Ltd. (APPC) for donating the salt cores for testing. The conclusions drawn in this study do not necessarily reflect the opinions of APPC.